Central European Science Journals
w w w . c e s j . c o m

Central European Journal of Physics
Central European Science Journals
CEJP 3 (2003) 485–515

Theoretical and experimental investigation of the photoacoustic effect in solids with residual stresses.

K.L. Muratikov*, A.L. Glazov

A.F.Ioffe Physical-Technical Institute of RAS,
194021 St.Petersburg, Polytechnicheskaya 26, Russia

Received 11 February 2003; revised 29 April 2003

Abstract: Modern experiment and theory in the field of residual stress detection by the photoacoustic method are summarized and analyzed. A multimode approach based on the simultaneous application of several photothermal and photoacoustic methods is proposed for the study of thermal and thermoelastic effects in solids with residual stress. Some experimental results obtained within the framework of this approach for Vickers indentation zones in ceramics are presented. The effect of annealing on the photoacoustic, piezoelectric signal for ceramics and the influence of the given external loading on the behavior of the photoacoustic signal near the radial crack tips is investigated. It is experimentally shown that both compressive and shear stresses contribute to the photoacoustic signal near the radial crack tips. The model of the photoacoustic, thermoelastic effect in solids with residual stress is proposed. It is based on the modified Murnaghan model of non-linear elastic bodies, which takes into account a possible dependence of the thermoelastic constant on stress. This model is further developed to explain the photoacoustic signal behavior near the radial crack tips. It is demonstrated that this model of the photoacoustic effect agrees qualitatively with the available experimental data.

Keywords: photoacoustics, residual stress, cracks, non-linear deformations, ceramics
PACS (2000): 62.20.-x, 62.30.+d, 65.49.De

1 Introduction

The presence of residual stresses both in bulk and on the surface of a material limits its strength and fatigue life. That is why at present much attention is paid to the problem of stress and residual stress detection in solids. The problem of residual and mechanical

* E-mail: klm@holo.ioffe.rssi.ru

stress detection in solids by the photoacoustic (PA) method has been investigated for about twelve years. The first PA detection of residual stress was made in the papers [1, 2]. Since then a number of similar applications of the PA effect [3]-[10] and electron-acoustic effect [11, 12] has been performed. In spite of these efforts, the PA methods are not widely used for residual stress detection up to now. This situation is essentially inconsistent with other methods such as optical [13], X-ray [14] and neutron [15] diffraction, ultrasound [16], Raman spectroscopy [17, 18], Stress Pattern Analysis by measurement of Thermal Emission (SPATE) [19], and the hole drilling method in conjunction with holographic or speckle interferometry [20], which are widely used for residual stress detection at present. Unfortunately, as a rule, these methods have rather limited fields of application. For example, optical methods are suitable only for transparent materials, Raman spectroscopy is mainly used in science and technology of semiconductors, for which the phonon lines have a relatively simple structure, and their shifts with stress are well known. SPATE and holographic interferometry are more generally applicable, but have comparatively low spatial resolution.

Of special interest are near-surface regions of solid materials and samples, where defects may result in excessively high operational and residual stresses. From this viewpoint, PA and photothermal (PT) methods are especially attractive for modern diagnostics and imaging [10]. These methods have micrometer resolution, are noncontact, and appear to be very useful for detection of cracks and voids, delaminations, and possible second phase material inclusions at microscopic and mesoscopic scales. The problem of residual stress and stress detection by these methods, however, has not been investigated profoundly. This situation, in our opinion, is primarily due to the lack of in-depth systematic studies of the PA effect in solids with residual stresses, including direct confirmation of residual stress effect on the PA signal. Therefore, the main purposes of this study were to summarize the available results and to prove substantial, direct evidence of a mechanical stress contribution to the PA signal.

2 Multimode set-up for photoacoustic and photothermal experiments

In the first investigations of the PA phenomena in solids with residual stresses, only the PA or electron-acoustic method was used. It is known that PA or electron-acoustic signals can depend on various thermal, thermoelastic, and elastic parameters of a sample under investigation. Therefore, in earlier investigations, it was impossible to control independently thermal, thermoelastic, and elastic parameters of an object, and to identify the origin of the effect observed. To overcome this restriction, we have proposed and applied in our work a multimode approach based on a simultaneous use of several PT and PA techniques [6]-[10]. It includes the PA gas microphone, photodeflection, photoreflectance, and PA piezoelectric measurements. The thermal properties in this approach are controlled and measured by the photodeflection, photoreflection and PA gas microphone methods, while the thermoelastic properties are controlled by the PA piezoelectric

method.

A multimode PT and PA microscope used in our experiments provides the PA gas microphone, photodeflection, photoreflectance, and PA piezoelectric measurements. The scheme of our set-up is shown in Fig.1. The images of the Vickers indented ceramics were obtained by scanning the samples along two coordinates with the step of 2.5 μm. The pump laser light was modulated in the range of frequencies from 100 Hz to 140 kHz. Thermal waves and acoustic vibrations were excited in the samples by the radiation of a continuous-wave argon-ion laser modulated by an acousto-optic modulator. The radiation of the pump laser was focused on a sample surface into an approximately 2 μm spot.

An important specific feature of our microscope is an opportunity to investigate the influence of external loading on the PA and PT responses in direct experiments with samples. It was possible in our experiments to apply external compressive loading in the direction parallel to the sample surface. The maximum loading was equal approximately to 2500 N. In our PA and PT experiments, it is possible to use samples with cross-sections of about several square millimeters. It means that our set-up provides an opportunity to perform experiments in a wide range of deformations, including plastic ones, for most of materials.

3 Experimental results of photothermal and photoacoustic study of modern ceramics with residual stresses

In this work, the experimental results are presented for hot-pressed silicon nitride (Norton Ceramic 132) and Al_2O_3-SiC-TiC ceramic (CRYSTALOY 2311 EDX). Residual stresses were introduced in ceramics by Vickers indentation, because indentation is one of the most reliable and reproducible methods for generation of residual stresses and crack systems in solids [21]. Samples were indented with loads from 49 N to 196 N. The average indentation diagonal on the sample surface at the load of 98 N was about 105 μm for hot-pressed silicon nitride ceramic and about 90 μm for Al_2O_3-SiC-TiC ceramics. Vickers indentation has a rather complicated structure. It includes core, plastic, and elastic zones, and radial or median cracks (see Fig.2). However, in this work, the main attention is paid to the investigation of the PA and PT signal behavior near the radial crack tips, where strong residual stresses are normally concentrated [22].

Let us consider results obtained in the different operating modes of the microscope, beginning with the PA piezoelectric one. The PA piezoelectric images were obtained for both hot-pressed silicon nitride and Al_2O_3-SiC-TiC ceramics. All these images, in general, have a similar structure. Therefore, we present here only the PA piezoelectric image of silicon nitride ceramic. The typical image of this type is shown in Fig.3. An important peculiarity of these images is the presence of regions with large signal amplitude located near the ends of the radial cracks. Previously, analogous features have been reported for the images of Vickers indentations obtained by electron-acoustic microscopy [2]. We have also observed this feature during the PA piezoelectric study of Al_2O_3-SiC-TiC ceramics [23, 24]. These PA images resemble to a great extent Raman microscopy images obtained

for the residual stress fields in Vickers-indented crystalline silicon [6]. Fig.4 shows a PA piezoelectric amplitude line scan along a radial crack. The cross represents the end of the radial crack visible at the surface.

The influence of stresses on thermophysical properties of metals was pointed out in an earlier investigation [1]. Therefore to clarify the dependence of thermal and elastic parameters of investigated ceramics on residual stress and its effect on the PA piezoelectric signal, we also analyzed thermal-wave images of the same regions by the PA gas microphone, photodeflection, and photoreflectance methods. In the photodeflection and photoreflectance modes of our microscope, the radiation of a He-Ne laser was used for readout. PA gas microphone and photodeflection measurements are sensitive only to thermal parameters of a sample [25]. A typical image obtained, for example, by photodeflection method for the case of the Vickers indented silicon nitride ceramic, is shown in Fig.5. Both amplitude and phase photodeflection images for this ceramic do not have any particular features near the radial crack tips.

Note that photodeflection images of Al_2O_3-SiC-TiC composite ceramic in general are similar to the presented images, with the exception of some additional speckle structure. However, this speckle structure is not determined by thermal or thermoelastic properties of this ceramic. It appears only due to different optical properties of Al_2O_3, SiC, and TiC grains of this ceramic. In our experiments with silicon nitride and Al_2O_3-SiC-TiC ceramics, we measured the photodeflection images of various Vickers indentations. In the experiments with silicon nitride, the detailed PA gas microphone and photoreflectance measurements were also made. In these experiments, we also did not observe any particular features near the radial crack tips in ceramics. Thus, our experimental results for ceramics lead to the conclusion that residual stresses do not noticeably influence their thermal properties.

When comparing various PT and PA images, note that the spatial resolution of the PT methods depends on both heating spot size and thermal wavelength. The heating spot size was the same in all the modes, whereas the thermal wavelength is inversely proportional to the square root of the modulation frequency. In silicon nitride ceramics it is, for example, about 10 mm at 100 kHz. In the PA gas microphone and photodeflection experiments, the modulation frequency is normally lower than 10 kHz, which reduces by several times the resolution of these methods compared to that of the PA piezoelectric method. This distinction hampers direct comparison of images obtained by these methods. The problem disappears using the photoreflectance method, operating in a very wide range of the modulation frequency.

In our experiments, photoreflectance images were obtained at modulation frequencies up to 140 kHz and were presented elsewhere [7]. Therefore, they can be compared directly with images obtained by the PA piezoelectric method at the same modulation frequency. Fig.6 shows the typical photoreflection image of a Vickers indentation zone in silicon nitride ceramic. In this image, the granular nature of the ceramic structure is demonstrated much more clearly than in PA gas microphone and photodeflection images. This characteristic is not caused by optical differences of the probe light reflection from different

grains, since the optical scanning image of this part of the ceramic, formed at the same time as the photoreflection image, was fairly homogeneous. This particular feature of the photoreflectance method is due to a special mechanism of its signal formation, based on the modulation of the photoreflectance coefficient by surface temperature. However, the photoreflection images, being sensitive to the modulation of the optical reflectance coefficient by the alternative temperature component, did not show any particular features near the ends of radial cracks. Thus, the PA gas microphone, photodeflection, and photoreflectance measurements of Vickers indentations in silicon nitride and Al_2O_3-SiC-TiC ceramics lead to the conclusion that residual stress does not noticeably influence its thermal parameters.

For more detailed investigation of the effect of residual stress on the PA piezoelectric signal, we have also measured the dependence of the signal on the load of indentation for silicon nitride ceramics. A typical dependence of the maximum of the PA piezoelectric signal at the crack ends on the indentation load for this ceramic is shown in Fig.7. The signal increases linearly with the load up to about 100 N, and then the signal growth decreases and the saturation takes place. For all obtained images, the PA piezoelectric signal from stressed regions does not exceed 160 percent of the signal from areas distant from indentations. The external stress produced by the load just before the saturation corresponds to the yield stress of this material near the radial crack tips. Under this condition, a further increase of the load does not result in the increase of residual stress in these regions, but in attainment of the critical stress for silicon nitride ceramic and only in a further radial crack growth.

In the previous studies of the PA effect in stressed materials, the PA response has not been investigated at additional external actions on objects such as temperature variation, loading, etc. The study of these effects can provide a direct demonstration of the existence of the dependence of the PA signal on residual stresses and ensure deeper understanding of this dependence. Therefore, in this work, we have also investigated the PA response from regions with residual stresses in ceramics under annealing and external loading.

Let us consider first the influence of annealing on the PA piezoelectric response from regions with residual stresses. For this purpose, we have measured the PA piezoelectric images of indentation sites after annealing of an Al_2O_3-SiC-TiC ceramic sample [23, 24]. Annealing was made at 800oC and was produced in three stages. The duration of each stage was equal to 8 hours. Note that after each annealing at 800oC, the sample temperature was decreased at a sufficiently slow rate (about 10oC/min) in order to minimize the effect of thermal stresses on the crack growth. In Fig.8 the maximum PA signal intensity normalized to the average PA response is shown within the course of annealing for two radial cracks in the Al_2O_3-SiC-TiC ceramic. Fig.8 reveals clearly a general tendency of the PA piezoelectric signal to decrease with increasing annealing time. For one of these cracks, some increase in the PA signal was observed after the 16-hour annealing. This event probably takes place because the regions of the material near crack tips are in a significantly nonequilibrium thermodynamic state [26], so that even weak thermal stresses can affect the crack growth. However, this event does not violate the general tendency.

The presented experimental data on the PA response variation in the course of annealing of the Al_2O_3-SiC-TiC ceramic are well consistent with the commonly accepted opinion that annealing decreases residual stress [26].

We have also made photodeflection imaging of an Al_2O_3-SiC-TiC ceramic sample after each stage of annealing to control its thermal properties. These experiments did not reveal any significant influence of annealing on the photodeflection images of Al_2O_3-SiC-TiC ceramics near Vickers indentations [23, 24]. Therefore, the results of photodeflection imaging both for silicon nitride and Al_2O_3-SiC-TiC ceramics show that the correlation between the PA piezoelectric response and residual stresses is not related to the effect of residual stresses on thermal properties of these materials or restoration of their thermal properties under annealing.

The second specific feature of this work is the investigation of the influence of external loading on the PA and PT responses in direct experiments with ceramics. Compressive external loading was applied in our experiments in the direction parallel to the sample surface. We have obtained the PA and PT images of Vickers indentations in unloaded and loaded Al_2O_3-SiC-TiC composite ceramic. First, it should be noted that the photodeflection images of Vickers indented areas in this ceramic do not demonstrate any influence of external loading. This fact correlates with the results of annealing experiments.

A typical modification of the PA piezoelectric image of the Vickers indented area in Al_2O_3-SiC-TiC composite ceramic under external loading is presented in Fig.9. From Fig.9 one can see that strong changes of the PA piezoelectric image with the application of external loading take place in various regions of the Vickers indented area, including the radial crack tips. This result can be considered as one more direct experimental proof of the PA piezoelectric signal dependence on mechanical stress. However, in this work, we restrict ourselves by the investigation of the PA signal behavior near the ends of radial cracks only. For interpretation of the PA experimental results in stressed materials, we developed a special theoretical model.

4 Theory of photothermal and photoacoustic thermoelastic problems for solids with residual stress

The detailed PT and PA study of solids with residual stress requires an adequate theoretical model. Novojilov [27] and Tokuoka et al [28], for example, give a general theoretical approach to the formulation of mechanical problems dealing with large elastic deformations and initially prestressed bodies. Some important details of the heat flux and thermoelastic problems for solids with large elastic deformations were discussed by Green et al [29]. Our main purpose is to develop, within the framework of these notions, the theoretical approach for the consideration of PT and PA effects in solids with residual stress.

Let us begin with the consideration of the heat flux problem. The derivation of the heat conduction equation can be started from the entropy flow equation in the general

form [30]

$$T\frac{\partial S}{\partial t} = div\vec{Q} + \rho W_H, \tag{1}$$

where S, T and ρ are the entropy, temperature, and density of a deformed body, $\vec{Q}$ is the heat flux in it, and W_H is the specific power of heat sources externally generated in the body.

In the mechanical model for an initially prestressed medium [27], the vector of positions of particles in the body in the final state is given by (see Fig.10)

$$\vec{R} = \vec{r} + \vec{U}(\vec{r}) + \Delta\vec{u}(\vec{r}, t), \tag{2}$$

where $\vec{r}$ gives positions of particles in the body in the natural state without stresses and $\vec{U}(\vec{r})$ denotes the static deformation of the body; $\Delta\vec{u}(\vec{r}, t)$ denotes small deformations caused by laser irradiation that are superimposed on the static deformation.

In our case, the generalized thermoelastic theory should be used [31]-[33]. It takes into account a possible dependence of thermoelastic coupling on strains. In the linear approximation of this parameter on initial strain, the density of the thermoelastic energy related to the deformation of the body from the initial state to the final one can be represented in the form

$$W_T = -\gamma_{ik}\left(u_{ik} - U_{ik}\right)\left(T - T_0\right), \tag{3}$$

where

$$\gamma_{ik} = \gamma_0\left[\left(1 + \beta_0 U_{pp}\right)\delta_{ik} + \beta_1 U_{ik}\right],$$

γ_0 is the thermoelastic coupling for an undeformed body, δ_{ik} is the Kronecker's delta function, β_0 and β_1 are the coefficients taking into account the dependence of the thermoelastic coupling on strain, $u_{ik} = \frac{1}{2}\left(\frac{\partial u_i}{\partial x_k} + \frac{\partial u_k}{\partial x_i} + \frac{\partial u_i}{\partial x_l}\frac{\partial u_k}{\partial x_l}\right)$is the strain tensor, U_{ik} is the initial strain tensor, and T_0 is the equilibrium temperature.

By analogy with the consideration made by Landau et al [30], we can determine the part of the entropy S of the initially isotropic body related to thermoelastic deformations of the body. Taking into account eq.(3), the entropy S of a body in the final state can be written as

$$S(\vec{R}, T, t) = S_0(\vec{U}, T) + \gamma_0\left[\left(1 + \beta_0 U_{pp}\right)\delta_{ik} + \beta_1 U_{ik}\right]\Delta u_{ik} \quad , \tag{4}$$

where $S_0(\vec{U}, T)$ is the entropy of the prestressed body and $\Delta u_{ik} = \frac{\partial \Delta u_i}{\partial x_k} + \frac{\partial \Delta u_k}{\partial x_i}$ is the tensor of small strain produced by modulated laser light.

The heat flux in a body can be expressed in a coordinate system corresponding to either its natural state or its initial state [29]. The thermal conductivity of materials is determined experimentally with regard to the natural coordinate system, because all lengths in the experiments of this type are normally measured in an undeformed material. The components of the heat flux vector in the prestressed body referred to the unit area of the undeformed body can be expressed as [29]

$$q_i = -K_{ik}\frac{\partial T}{\partial x_k}. \tag{5}$$

In this relation the thermal conductivity tensor K_{ik} in a general, non-linear, thermoelastic theory can be expressed in terms of invariants composed from strain tensor, temperature, and temperature gradients [34].

The heat flux vector $\vec{q}$is expressed in terms of Lagrange's coordinates x_i, while the heat flux vector $\vec{Q}$ in eq.(1) is given in terms of Euler's coordinates. Using transformations described in [29], for example, one can express all values in Lagrange's coordinates. From eqs.(1), (4), and (5) one can then derive the heat conduction equation for the prestressed body. In this work, we suppose that both temperature modulation ΔT and deformations Δu_i are small. In the linear approximation the heat conduction equation can then be represented in the form

$$\rho_0 c_v \frac{\partial \Delta T}{\partial t} + \gamma_0 T_0 \frac{\rho_0}{\rho} \Big[(1 + \beta_0 U_{pp})\, \delta_{ik} + \beta_1 U_{ik} \Big] \frac{\partial \Delta u_{ik}}{\partial t} = \frac{\partial}{\partial x_i} \left(K_{ik} \frac{\partial \Delta T}{\partial x_k} \right) + \rho_0 W_H, \quad (6)$$

where ρ_0 is the density of the undeformed body andc_v is the specific heat of the prestressed body at a constant volume.

All values in eq.(6) are expressed in terms of Lagrange's coordinates x_i corresponding to positions of points of the undeformed body. The second term in the left side of eq.(6) is related to dilatation processes and influences weakly the temperature distribution determined by a thermal diffusion process, though it plays an important role in investigation of thermal infrared emission effects by the SPATE technique [19]. This term is usually omitted in the PT and PA problems. eq.(6) shows that the temperature distribution in the deformed body varies with initial stresses via the density, thermal conductivity, and specific heat. For our problem, only the dependence of these values on the initial strain is essential.

In the linear approximation on the initial strain tensor, these values can be written as

$$\begin{aligned} c_v &= c_v^{(0)}\, (1 + \delta U_{pp})\,, \\ \rho &= \rho_0\, (1 - U_{pp})\,, \\ K_{ik} &= K_0\, [(1 + \varepsilon_0 U_{pp})\, \delta_{ik} + \varepsilon_1 U_{ik}]\,, \end{aligned} \quad (7)$$

where $c_v^{(0)}$and K_0 are the specific heat and thermal conductivity of the undeformed body, respectively;δ, ε_0, and ε_1 are the coefficients taking into account the dependence of the specific heat and thermal conductivity on strain.

For the case $\rho = \rho_0$, $\beta_0 = \beta_1 = 0$ and $K_{ik} = K_0 \delta_{ik}$ eq.(6) coincides with a well known heat conduction equation for isotropic bodies [30].

For the formulation of the complete thermoelastic problem for bodies with residual stress it is necessary to add to eq.(6) an equation for determination of deformations Δu_i. This equation can be obtained within the framework of non-linear mechanics using the equation of motion for a body [27, 34]. In the absence of external forces, the equation of motion is given by

$$\frac{\partial P_{ik}}{\partial x_k} = \rho_0 \frac{\partial^2 \Delta u_i}{\partial t^2}, \quad (8)$$

where $P_{ik} = \frac{\partial X_i}{\partial x_m}\frac{\partial W}{\partial u_{km}}$ is Piola-Kirchhof's stress tensor; X_i are the coordinates of vector $\vec{R}$, i.e., Euler's coordinates of particles in the deformed body; $u_{km} = U_{km} + \Delta u_{km}$; and$W$ is the total energy density function.

The total energy density W can be represented in the form $W = W_E + W_T$, where W_E is the density of the mechanical energy and W_T is the change of the Helmholtz free energy of the body related to its deformation from the initial state to the final state, which is determined by eq.(3).

In this paper, it is supposed that in the natural state the body is isotropic, and its mechanical energy is represented by the Murnaghan non-linear, mechanical model of the body [35]. In accordance with this model the density of elastic energy of the body under deformations can be expressed in the form

$$W_E = \Big(\lambda + 2\mu\Big)\frac{I_1^2}{2} - 2\mu I_2 + \Big(l + 2m\Big)\frac{I_1^3}{3} - 2mI_1I_2 + nI_3, \tag{9}$$

where λ and μ are Lame's elastic constants; l,m,n are the third order Murnaghan constants; I_1, I_2, and I_3 are the three invariants of the strain tensor [35]. The third order Murnaghan constants are unambiguously related to the third-order elastic modulii of material [35].

The general solution of the formulated problem has serious mathematical difficulties. Therefore, in this work, it is assumed that the static deformations in the prestressed body are homogeneous and can be represented in the form $U_i = A_i x_i$ ($A_i = \text{const}$). Let us also assume that the sample surface is uniformly irradiated by laser light temporary modulated according to the harmonic law, and that the dilatation processes do not influence the temperature inside the body. Under these conditions, the one-dimensional model can be used for thermal waves and elastic deformations in the body.

To obtain a solution of eq.(8), it is necessary to know a distribution of the alternative temperature component inside the object. For the laser light fully absorbed at the top sample surface, under the above assumptions, and by using eqs.(6) and (7), one can express the alternative temperature component for a thermally thick sample as

$$\Delta T\,(z,t) = \Delta T_s(\omega)e^{-\sigma z + i\omega t}, \tag{10}$$

where $\sigma = (1+\iota)\sqrt{\frac{\omega}{2\kappa}}$, $\kappa = \kappa_0\frac{(1+\varepsilon_0 U_{pp})+\varepsilon_1 U_{33}}{1+\delta U_{pp}}$, κ_0 is the thermal diffusivity of the undeformed body, ΔT_S is the amplitude of the temperature modulation on the sample surface, ω is the angular frequency of laser beam modulation, and the z axis is directed perpendicular to the sample surface.

In our work, the piezoelectric element was used for the detection of sample vibrations (see Fig.11). Under conditions of our experiments, the length of acoustic waves in the piezoelectric element was longer than its thickness. Therefore, the deformation of the piezoelectric element can be considered as homogeneous. The output voltage of electric signal $V(\omega)$ produced by the piezoelement can then be written as [34]

$$V(\omega) = -\frac{e^{(T)}}{\varepsilon^{(ST)}} l_1 \frac{\partial u_3^{(p)}(z,\omega)}{\partial z}\Big|_{z=l}\,, \tag{11}$$

where l_1 is the thickness of the piezoelement, $u_3^{(p)}(z,\omega)$ is the deformation of the piezoelectric element, and $e^{(T)}$ and $\varepsilon^{(ST)}$ are the piezoelectric and dielectric constants of the piezoelectric material respectively.

The deformation of the piezoelement $u_3^{(p)}(z,\omega)$ can be related to the sample deformation $\Delta u_3(z,\omega)$ using the condition of the normal stress component continuity at the boundary between the sample and the piezoelement

$$t_{33}^{(p)} = P_{33}\,|_{z=l}\,, \tag{12}$$

where $t_{33}^{(p)}$ is the mechanical stress inside the piezoelement.

The scheme of the derivation of deformations Δu_i from thermoelastic equation (8) was described elsewhere [31]-[33], where the linearization procedure for eq.(8) was developed. Therefore, in this paper we do not consider this procedure in detail. After linearization, one can rewrite the equation of motion for our case in the form

$$f_k^{(i)}\frac{\partial^2\Delta u_i}{\partial x_k\partial x_k} + h_k^{(i)}\frac{\partial^2\Delta u_k}{\partial x_k\partial x_i} = g^{(i)}\frac{\partial\Delta T}{\partial x_i} + \rho_0\Delta\ddot{u}_i \quad , \tag{13}$$

where $f_k^{(i)}$, $h_k^{(i)}$, and $g^{(i)}$ are the coefficients defined in the same manner as in [31]-[33], and the summation over the subscript k in the left side of eq.(13) is assumed.

One can obtain the deformations of a sample with the free top surface using the boundary condition

$$n_k P_{ik}\,\big|_{z=\Delta u_3} = 0, \tag{14}$$

where n_k are the components of the unit vector normal to the sample surface.

For a massive piezoelectric transducer that is much heavier than the sample used in our experiments, we can assume that the displacement of sample points at the boundary between the sample and the element obeys the equation $\Delta u_3(l,\omega) = 0$. In this work, it is assumed also that the alternative temperature ΔT_s and deformation Δu_3 components are small. Boundary condition (14) can then be simplified, because in the first order approximation on these values, the equation $z = \Delta u_3$ can be replaced by $z = 0$.

For the given boundary conditions, the solution of eq.(13) $\Delta u_3(z,\omega)$ for the one-dimensional model can be obtained in the form

$$\Delta u_3\,(z,\omega) = U_3^{(0)}\left(\frac{Q}{\sigma}\frac{\sin Q\,(z-l)}{\cos Ql} - e^{-\sigma z} + e^{-\sigma l}\frac{\cos Qz}{\cos Ql}\right), \tag{15}$$

where $U_3^{(0)} = \frac{\gamma_0\sigma(1+A_3)(1+\beta_0U_{pp}+\beta_1U_{33})}{\left(f_3^{(3)}+h_3^{(3)}\right)\sigma^2+\rho_0\omega^2}\Delta T_s$ and$Q = \sqrt{\frac{\rho_0\omega^2}{f_3^{(3)}+h_3^{(3)}}}$.

In our experiments, relatively low modulation frequencies of the pump beam were used, which obey the condition $\kappa\omega \leqslant c_l^2$ (where c_l is the longitudinal velocity of sound in the body). Based on Eqs.(11), (12), and (15), the PA piezoelectric signal $V(\omega)$ for this case can be represented in the following form

$$V(\omega) = V_0(\omega)\frac{\sqrt{1+\varepsilon_0U_{pp}+\varepsilon_1U_{33}}}{\left[(1-U_{pp})\,(1+\delta U_{pp})\right]^{3/2}} \times\frac{1+\beta_0U_{pp}+\beta_1U_{33}}{\sqrt{1+A_3}\left[1+2l\textcircled{c}U_{pp}+(4m\textcircled{c}+n\textcircled{c})U_{33}\right]^{3/2}}, \tag{16}$$

where $V_0(\omega)$ is the PA piezoelectric signal from the undeformed body, $l' = l/(\rho_0 c_l^2)$, $m' = m/(\rho_0 c_l^2)$,$n' = n/(\rho_0 c_l^2)$, and $\rho_0 c_l^2 = K + 4/3\mu$, where K andμ are the modulii of elasticity and shift respectively.

This result is of a general nature and can be applied for various materials. It relates the dependence of the PA piezoelectric signal on stress or strains to the non-linear thermal, thermoelastic, and elastic properties of a material. Note that this result must be valid also for the electron-acoustic signal when special details of thermal wave generation by the electron beam are not important. This fact may explain the great similarity between the PA [3, 4, 6] and electron-acoustic [2],[11]-[13] images of areas near Vickers indentations.

An analysis of the obtained experimental and theoretical results can be performed. First of all, from the PA gas microphone, photodeflection, and photoreflectance data, one concludes that ε_0, ε_1 and δ are about zero for investigated silicon nitride (Norton Ceramic 132) and Al_2O_3-SiC-TiC (CRYSTALOY 2311 EDX) ceramics. Using the expression for the PA piezoelectric signal and experimental results, we can also make some estimation of the coefficients (β_0, β_1) and the Murnaghan constants of these ceramics. In accordance with these experimental results, the maximal PA piezoelectric signal from the stressed areas in silicon nitride and Al_2O_3-SiC-TiC ceramics exceeds the average signal by 40-60 percent. Young's modulus and shear modulus for silicon nitride ceramic are given, for example, by Sharma et al [36] and are equal to 320 GPa and 130 GPa respectively. Therefore, according to the developed theory, these experimental results, and the maximal possible values of strains in ceramics [37], we can estimate the values of the Murnaghan constants as $(3 \div 10)\times 10^{12}$ Pa for silicon nitride ceramic and the upper values of the coefficients (β_0, β_1) as $5 \div 10$ for both ceramics. The estimated values of the Murnaghan constants lie in the correct range of these parameters for solids presented, for example, by Lur'e [38]. The coefficients (β_0, β_1) have somewhat larger values with reference to the values estimated by Garber et al [39] for metals. However, in this estimation, only the influence of stresses on the coefficient of thermal expansion was taken into account. The inclusion of the non-linear elastic effects into consideration can somewhat change this estimation. Unfortunately, more accurate determination of these parameters requires the development of special experimental procedures and additional theoretical studies.

5 Theoretical model of photoacoustic thermoelastic effect near vertical crack tips

We have presented experimental results demonstrating the influence of mechanical stresses on the PA and electron-acoustic signals near the radial crack tips of Vickers indentations in ceramics. We have also presented the theoretical model of the PA and electron-acoustic effect in stressed materials. Up to now, however, there was no proposed theoretical model to explain the PA signal behavior near the crack tips. Therefore, we developed further the described model of the PA effect in stressed solids to explain the PA and electron-acoustic signal peculiarities near the radial crack tips of Vickers indentations [40].

To apply our theoretical model of the PA effect in stressed solids to determine the

PA signal behavior near the radial crack tips, it is necessary to take into account several specific features of the PA and electron-acoustic experiments with Vickers indentations. First, in these experiments, the PA or electron-acoustic signals are usually generated in a relatively thin subsurface layer. Therefore, the depth of the radial cracks in these experiments exceeds the thickness of this layer. In our investigation, we took into account that residual strains in brittle materials are small except for plastically deformed regions. We took also into account that residual stresses near the tips of radial cracks are directed mainly parallel to the sample surface. Therefore, one can assume that in PA experiments for components of the strain tensor U_{ik} produced by residual stresses, it must be true that $U_{ik} << 1$ and U_{xx},$U_{yy} >> U_{zz}$, where z-axis is directed perpendicular to the sample surface. For this case, the PA signal in accordance with eq.(16) can be expressed in the linear on residual strains approximation in the form

$$\Delta V(\omega) = \Delta A(U_{xx} + U_{yy}), \tag{17}$$

where $A = V_0(\omega)(\beta_0 + 3/2 - 3l')$, $V_0(\omega)$ is the PA piezoelectric signal from the undeformed body, $l' = \frac{l}{\rho_0 c_l^2}$, l is the third order Murnaghan constant, ρ_o is the density of the undeformed body, $c_l$is the longitudinal velocity of sound, and β_0 is the coefficient taking into account the dependence of the thermoelastic coupling on strains [19], [31]-[33].

Small plastically deformed regions at the crack ends are localized near the radial crack tips. The regions with residual stresses occupy essentially larger areas. In these areas, residual strains have elastic character, and they can be expressed through residual stresses by using Hooke's law. In accordance with eq.(17) the PA signal can then be represented in the form

$$\Delta V(\omega) = A'(\sigma_{xx} + \sigma_{yy}), \tag{18}$$

where $A' = \frac{1-\nu}{E}A$, ν is Poisson's ratio, E is Young's modulus, and σ_{xx} and σ_{yy} are the components of the stress tensor.

First, note that the dependence of the PA signal on stress is determined by the same values as in the case of stress pattern analysis by measurement of thermal emission (SPATE) method. In accordance with paper [19] the SPATE signal is also proportional to $\sigma_{xx} + \sigma_{yy}$.

It was already pointed out that in the PA and electron-acoustic experiments, the thin surface layer was responsible for the formation of the PA signal. In this case, for the determination of residual stresses near the radial crack tips, these cracks can be considered as plane ones. The components of the stress tensor near the plane crack tip in a thick sample are determined by equations [22]

$$\begin{aligned}\sigma_{xx} = {} & \frac{K_I}{\sqrt{2\pi r}} \cos\frac{\theta}{2}\left(1 - \sin\frac{\theta}{2}\sin\frac{3\theta}{2}\right) \\ & -\frac{K_{II}}{\sqrt{2\pi r}} \sin\frac{\theta}{2}\left(2 + \cos\frac{\theta}{2}\cos\frac{3\theta}{2}\right),\end{aligned} \tag{19a}$$

$$\sigma_{yy} = \frac{K_I}{\sqrt{2\pi r}} \cos\frac{\theta}{2}\left(1 + \sin\frac{\theta}{2}\sin\frac{3\theta}{2}\right) + \frac{K_{II}}{\sqrt{2\pi r}} \sin\frac{\theta}{2}\cos\frac{\theta}{2}\cos\frac{3\theta}{2}, \tag{19b}$$

where K_I and K_{II} are the stress intensity factors that define the normal and shear components of stress produced by external loading, r is the distance between the crack tip and the point of measurement, and θ is the angle between the crack and direction of the point of measurement.

The stress intensity factors of the crack in the general case are determined by the total action of residual stresses and stresses produced by external loading. In linear crack mechanics, the total stress intensity factors of a crack can be represented in the form

$$\begin{aligned} K_I &= K_I^{(0)} + K_I^{(1)}, \\ K_{II} &= K_{II}^{(0)} + K_{II}^{(1)}, \end{aligned} \tag{20}$$

where$K_I^{(0)}$ and $K_{II}^{(0)}$ are the stress intensity factors related to residual stresses and $K_I^{(1)}$ and $K_{II}^{(1)}$ are the stress intensity factors characterizing the crack behavior under external loading.

The stress intensity factors that take into account the external loading of a crack depend both on the value of this loading and on the angle between the crack and external stress direction (see Fig.12). For the case of the plane crack, these stress intensity factors are determined by equations [41]

$$\begin{aligned} K_I^{(1)} &= K_I^{(1)'} \sin^2\phi, \\ K_{II}^{(1)} &= K_{II}^{(1)'} \sin\phi\cos\phi, \end{aligned} \tag{21}$$

where ϕ is the angle between the crack and direction of the external loading and K_I' and K_{II}' are the stress intensity factors that characterize the crack and do not depend on the angle ϕ.

Let us consider in more detail the PA signal behavior near the radial crack tips of Vickers indentation under external loading by using the obtained results. The stress intensity factors of the radial cracks for residual stresses produced by Vickers indentation are given by expressions [42]

$$\begin{aligned} K_I^{(0)} &= \chi\frac{P}{L^{3/2}}, \\ K_{II}^{(0)} &= 0, \end{aligned} \tag{22}$$

where P is the indentation loading, χ is the dimensionless coefficient whose value is determined by the shape of a crack, and L is the length of a crack.

Using Eqs.(18-22) the PA signal near the radial crack tips can be expressed in the form

$$\Delta V(\omega) = A'\sqrt{\frac{2}{\pi r}}\left[\left(K_I^{(0)} + K_I^{(1)'}\sin^2\phi\right)\cos\frac{\theta}{2} - K_{II}^{(1)'}\sin\phi\cos\phi\sin\frac{\theta}{2}\right]. \tag{23}$$

Equation (23) can be used to determine the influence of external stresses on the PA signal. To perform this comparison, we have analyzed in this work the behavior of the PA signal near the tip of a crack in directions perpendicular to a crack direction. The choice of these directions was determined by the fact that the distribution of normal and shear stresses along them has an essentially different character under loading.

Fig.13 demonstrates the experimental data representing the behavior of the PA signal along the described directions for two radial cracks in Al_2O_3-SiC-TiC composite ceramic. Theoretical results obtained from eq.(23) are also presented in this figure. The chosen cracks denoted as 1 and 4 in Fig.9 correspond to the situation in which the impact of the external loading on the stress fields near crack tips has a quite different character. For crack 1 the angle $\phi \cong 75^0$, and external loading is almost normal to the crack interfaces. For crack 4 the angle $\phi \cong 17^0$, and external loading produces nearly pure shear stress. In the theoretical calculations, the distances between the crack tip and the line of the PA scanning were 5 μm for crack 1 and 20 μm for crack 4. The results presented in Fig. 13 demonstrate a good agreement of the experimental data with our theoretical model at short distances from the crack tips. Some disagreement between experimental and theoretical results at distances away from the crack tips is due to an asymptotical character of the expressions used for stress tensor components [41] that are valid only for short distances. Fig.13(a) shows that external compressive stress partially compensates for tensile residual stress acting near the tip of crack 1.

The proposed theoretical model, in combination with experimental data for Al_2O_3-SiC-TiC ceramic, enables us to make some conclusions about the stress intensity factors of the radial cracks in this material. To perform this analysis, it is necessary to take into account eq.(22). The stress intensity factor related to the applied external loading for a crack with $\phi = 90^0$ is determined by expression $K_I^{(1)'} = \psi\sigma\sqrt{L}$, where ψ is another dimensionless coefficient whose value is also determined by the crack shape and σ is the external uniform tension perpendicular to the crack plane [42]. From the experimental data shown in Fig.6 of paper [40], it is evident that the compensation for tensile residual stresses near the tips of radial crack with $\phi = 90^0$ takes place under the external compressive stress equal approximately to 340 MPa. The radial crack length in the Al_2O_3-SiC-TiC composite generated by Vickers indentation at 98 N was equal to about 150 μm. The experimental data and results in eq.(23) for the PA signal then make it possible to obtain a constraint on the coefficients χ and ψ. From our data, one can conclude that $\chi \cong 0.075\psi$. Note that this estimation is in good quantitative agreement with the result obtained in paper [43] for ceramics with Al_2O_3 grains. One can also conclude from the theoretical and experimental results obtained here that $K_I^{(1)'} \cong K_{II}^{(1)'}$. The last result is in good agreement with the theory of plane cracks in thick plates [41], which gives the exact equality for these values. Therefore the experimental data that are related to the PA signal behavior near the crack tips, in combination with the theoretical results of the crack mechanics, enable us to make some conclusions about the stress intensity factors of radial cracks in the Al_2O_3-SiC-TiC composite ceramic.

The theoretical model developed here demonstrates the substantial influence of the

external loading on the PA piezoelectric signal near Vickers indentations. The modifications of the PA signal obtained here show that they reproduce both normal and shear stresses near the ends of the radial cracks. It is demonstrated that the theoretical results presented here, in combination with available data of PA experiments with Vickers indentations, can be used for extracting important information about the stress intensity factors of the radial cracks.

6 Conclusion

The approach proposed in this work could provide both the experimental and theoretical base for the investigation of stress and residual stress influence on thermal and thermoelastic properties of materials. To our mind, it would be interesting to apply this approach for experimental investigations of the dependence of thermal parameters on stress for different materials. The PT data presented in this work do not show any strong influence of stress on thermal properties of the silicon nitride and Al_2O_3-SiC-TiC ceramics. However, there is no reason to generalize this result to other types of materials. The experimental results obtained in the field of the PA effect could be used for the measurement of thermoelastic and Murnaghan constants (or third order elastic modulii) of materials by PA techniques.

The residual stress fields for Vickers-indented regions have a rather complicated structure. This obstacle essentially limits the application of the PA techniques for quantitative measurements of non-linear thermoelastic and elastic parameters. Therefore, the development of specialized PT and PA techniques based on the use of samples with a simple structure of residual stresses could be of great importance.

The non-linear thermoelastic theory of the PA effect in solids with residual stresses developed in this work is of a general character and can be applied to various materials. This theory can describe the main features of the thermoelastic generation of acoustic vibrations in solid objects. It provides a qualitative explanation of the experimental data obtained here and can be applied to the case of the electron-acoustic microscopy, when special details of thermal wave generation by the electron beam are not essential. It is shown also that this theory relates the PA piezoelectric signal to stresses in the form analogous to the SPATE signal. The detected behavior of the PA signal reproduces both normal and shear stresses near the ends of radial cracks in accordance with the proposed theoretical model. In combination with the presented theoretical, results the experimental PA data can be used for extracting important information about the stress intensity factors of cracks.

In this work, the expressions for the PA piezoelectric signals have been obtained within the framework of the one-dimensional model. More realistic, three-dimensional models of the PA piezoelectric signal formation that take into account actual features of the residual stress fields are, therefore, of great interest. These models could provide a better agreement between experimental and theoretical results.

The dependence of the PA thermoelastic signal on residual stresses provides an in-

teresting opportunity for the development of new, nondestructive methods for residual stress detection in solids. In this case, the general applicability and the capability of providing better spatial resolution, compared to the holographic interferometry and SPATE methods, could be the important advantages of these methods.

Acknowledgments

This work was partially supported by Russian Foundation for Basic Research under Grant No.01-01-00855 and the U.S. Civilian Researc & Development Foundation for the Independent States of the Former Soviet Union (CRDF) under Award No.RP1-2366-ST-02.

References

[1] M. Kasai and T. Sawada: "Non-destructive Evaluation of the Distribution of Stress by Means of the Photoacoustic Microscopy", In: *Photoacoustic and Photothermal Phenomena.*, II edited by J.C.Murphy, J.W. Maclachlan Spicer, L.C. Aamodt and B.S.H. Royce, Springer-Verlag, Berlin, Vol. 62, 1990, pp. 33–36.

[2] J.H. Cantrell, M. Qian, M.V. Ravichandran, K.M. Knowles: "Scanning Elctron Acoustic Microscopy of Indentation - Induced Cracks and Residual Stresses in Ceramics", *Appl.Phys.Lett.* Vol. 57, (1990), pp. 1870.

[3] R.M. Burbelo, A.L. Gulyaev, L.I. Robur, M.K. Zhabitenko, B.A. Atamanenko, Ya.A. Kryl: "Photoacoustic Visualization of Residual Stress in Ceramic Materials", *J. de Phys. 4*, Vol. C7, (1994), pp. 311.

[4] H. Zhang, S. Gissinger, G. Weides, U. Netzelman: "Detection of Surface Damage in Ceramic by Photothermal and Photoacoustic Techniques", *J. de Phys. 4*, Vol. C7, (1994), pp. 603.

[5] R.M. Burbelo and M.K. Zhabitenko: "Photoacoustic effect in Elastic Stressed Regions of Solids", In: *Progress in Natural Science*, edited by Shu-yi Zhang, Taylor & Francis, London and Washington, Suppl., Vol. 6, 1996, pp.720–723.

[6] K.L. Muratikov, A.L. Glazov, D.N. Rose, J.E. Dumar, G.H. Quay: "Photodeflection and photoacoustic mycroscopy of cracks and residual stresses induced by Vickers indentation in silicon nitride ceramic", *Tech. Phys. Lett.*, Vol. 23, (1997), pp. 188.

[7] K.L. Muratikov, A.L. Glazov, D.N. Rose, J.E. Dumar: "Investigation of the Influence of Residual Stresses on the Thermophysical and Thermoelastic Properties of Silicon Nitride Ceramic by Photothermal and Photoacoustic Methods", *Tech. Phys. Lett.*, Vol. 24, (1998), pp.846.

[8] K.L. Muratikov, A.L. Glazov, D.N. Rose, J.E. Dumar: "Photoacoustic Effect in Stressed Elastic Solids", it J. Appl. Phys., Vol. 88, (2000), pp. 2948.

[9] K.L. Muratikov, A.L. Glazov, D.N. Rose, J.E. Dumar: "On the Possibility of Photoacoustic and Photothermal Detection of Residual Stresses in Solid Materials. Proceedings of the 6th International Conference on Residual Stresses", In: *Proceedings of the 6th International Conference on Residual Stresses*, IOM Communications, Vol. 1, London, 2000, pp.641-648.

[10] K.L. Muratikov, A.L. Glazov, D.N. Rose, J.E. Dumar: "Photothermal and Photoacoustic Measurement of Thermal and Thermpelastic Properties of Ceramics with Residual Stresses", *High Temperatures - High Pressures*, Vol.33, (2001), pp. 285.

[11] F. Jiang, S. Kojima, B. Zhang, Q. Yin: "Some New Applications of the Scanning Electron Acoustic Microscope for Materials Evaluation", *Jpn. J. Appl. Phys.*, Vol. 37(5B), (1998), pp. 3128.

[12] Y. Gillet and C. Bissieux: "Vickers Indentation Imaging by Scanning Electron Acoustic Microscopy", *Abstract of the 10th International Conference on Photoacoustic and Photothermal Phenomena*, Rome(Italy), 23–27 August 1998, pp.131-132.

[13] A.Ya. Aleksandrov and M.Kh. Akhmetayanov: *Polarization Optical Methods in Mechanics of Deformable Bodies*, Nauka, Moscow, 1974.

[14] B. Eigenmann, B. Scholtes, E. Macherauch: "Determination of Resudual Stresses in Ceramics and Ceramic-Metal Composites by X-ray Diffraction Methods", *Mater. Sci. Eng.*, Vol. A118, (1989), pp. 1.

[15] M.R. Daymond, M.A.M. Bourke, R.B. Von Dreele, B. Clausen, T. Lorentzen: "Use of Rietveld Refinement for Elastic Macrostrain Determination and for Evaluation of Plastic Strain History from Diffraction Spectra", *J. Appl. Phys.*, Vol. 82, (1997), pp. 1554.

[16] Y.H. Pao, W. Sachse, H. Fukuoka: "Acoustoelasticity and ultrasonic measurements of residual stress", In: *Physical Acoustics*, edited by W.P. Mason and R.N. Thurston, Academic Press, New York, Vol. 17, 1984, pp. 61–143.

[17] T. Iwaoka, S. Yokoyama, Y. Osaka: "A New Method of Measuring Internal Stress in Thin Films Deposited on Silicon by Raman Spectroscopy", *Jpn. J. Appl. Phys.*, Vol. 24, (1985), pp. 112.

[18] M. Bowden and D.J. Gardiner: "Stress and Structural Images of Microindented Silicon by Raman Microscopy", *Appl. Spectrosc.*, Vol. 51, (1997), pp. 1405.

[19] A.K. Wong, R. Jones, J.G. Sparrow: "Thermoelastic Constant or Thermoelastic Parameter?", *J. Phys. Chem. Solids.*, Vol. 48, (1987), pp. 749.

[20] D.R. Schmitt and Y. Li: "Three-dimentional Stress Relief Displacement Resulting from Drilling a Blind Hole in Acrylic", *Exp. Mech.*, Vol. 36, (1996), pp. 412.

[21] R.F. Cook and G.M. Pharr: "Direct Observation and Analysis of Indentation Cracking in Glasses and Ceramics", *J. Am. Ceram. Soc.*, Vol. 73, (1990), pp. 787.

[22] B.R. Lawn: *Fracture of Brittle Solids*, Cambridge University Press, Cambridge, 1993.

[23] K.L. Muratikov, A.L. Glazov, V.I. Nikolaev, D.N. Rose, J.E. Dumar: "The Effect of Annealing on the Photoacoustic and Photothermal Response of Al2O3-SiC-TiC Ceramics with Internal Stresses", *Tech. Phys. Lett.*, Vol. 27, (2001), pp. 33.

[24] K.L. Muratikov, A.L. Glazov, D.N. Rose, J.E. Dumar: "Photoacoustic Thermoelastic Effect in Ceramics with Residual Stresses under Annealing", In: *Proceedings of the 4th International Congress on Thermal Stresses.*, Osaka, Japan, 8-11 June 2001, pp. 85–88.

[25] A.C. Tam: "Applications of Photoacoustic Sensing Techniques", *Rev. Mod. Phys.*, Vol. 58, (1986), pp. 381.

[26] V.S. Ivanova, A.S. Balankin, I.J. Bunin, A.A. Oksogoev: *Synergetics and Fractals in Material Science*, Nauka, Moscow, 1994.

[27] V.V. Novojilov: *Foundations of the Nonlinear Theory of Elasticity*, Glaylock Press, Rochester and New York, 1953.

[28] T. Tokuoka and M. Saito: "Elastic Wave Propagations and Acoustical Birefringence in Stressed Crystals', *J. Acoust. Soc. Am.*, Vol. 45, (1968), pp. 1241.

[29] A.E. Green and J.E. Adkins: *Large Elastic Deformations and Non-linear Continuum Mechanics*, Clarendon Press, Oxford, 1960.

[30] L.D. Landau and E.M. Lifshitz: *Theory of Elasticity*, 3rd ed., Pergamon, Oxford, 1986.

[31] K.L.Muratikov: "Theory of the Thermoelastic Generation of Mechanical Vibrations in Internally Stressed Solids by Laser Radiation", *Tech. Phys. Lett.*, Vol. 24, (1998), pp. 536.

[32] K.L. Muratikov: "Theory of the Thermoelastic Laser Induced Deformations in Solids with Residual Stresses", In: *Proceedings of the 10th International Conference on Photoacoustics and Photothermal Phenomena edited by F. Scudiery and M. Bertolotti (AIP Conference Proceedings 463*, Woodbury, New York, 1998, p. 478.

[33] K.L. Muratikov: "Theory of Generation of Mechanical Vibrations by Laser Radiation in Solids Containing Internal Stresses on the Basis of the Thermoelastic Effect", *Tech. Phys.*, Vol. 44, (1999), pp. 792.

[34] M. Qian: "New Thermoelastic Technique for Detection of Residual Stress Distribution in Solids", *Chinese J. Acoust.*, Vol. 14, (1995), pp. 97.

[35] F.D. Murnaghan: *Finite Deformation of an Elastic Solid*, Wiley, New York, 1951.

[36] V. Sharma, S. Nemat-Nasser, K.S. Vecchio: "Effect of Grain-Boundary Phase on Dynamic Compression Fatigue in Hot-Pressed Silicon Nitride", *J. Am. Ceram. Soc.*, Vol. 81, (1998), pp. 129.

[37] T.J. Mackin and T.E. Purcell: "xxx", *Exp. Techniques*, Vol. 20, (1996), pp. 15.

[38] A.I. Lur'e: *Nonlinear Theory of Elasticity*, North-Holland, Amsterdam, 1990.

[39] R.I. Garber and I.A. Gindin: "Elastic Deformation and Thermal Expansion", *Sov. Phys. Solid State*, Vol. 3, (1961), pp. 127.

[40] K.L. Muratikov, A.L. Glazov, D.N. Rose, J.E. Dumar: "The Effect of Mechanical Loading on the Photoacoustic Response from Radial Cracks in Vickers-Indented Al2O3-SiC-TiC Ceramics", *Tech. Phys. Lett.*, Vol. 28, (2002), pp. 377.

[41] L.M. Sedov: *Mechanics of Continuous Medium*, Nauka, Moscow, 1970.

[42] S.M. Smith and R.O. Scattergood: "Crack-Shape Effects for Indentation Fracture Toughness Measurements", *J.Am.Ceram.Soc.*, Vol. 75, (1992), pp. 305.

[43] L.M. Braun, S.J. Bennison, B.R. Lawn: "Objective Evaluation of Short Crack Toughness Curves Using Indentation Flaws: Case Study on Alumina-Based Ceramics", *J.Am.Ceram.Soc.*, Vol. 75, (1992), pp. 3049.

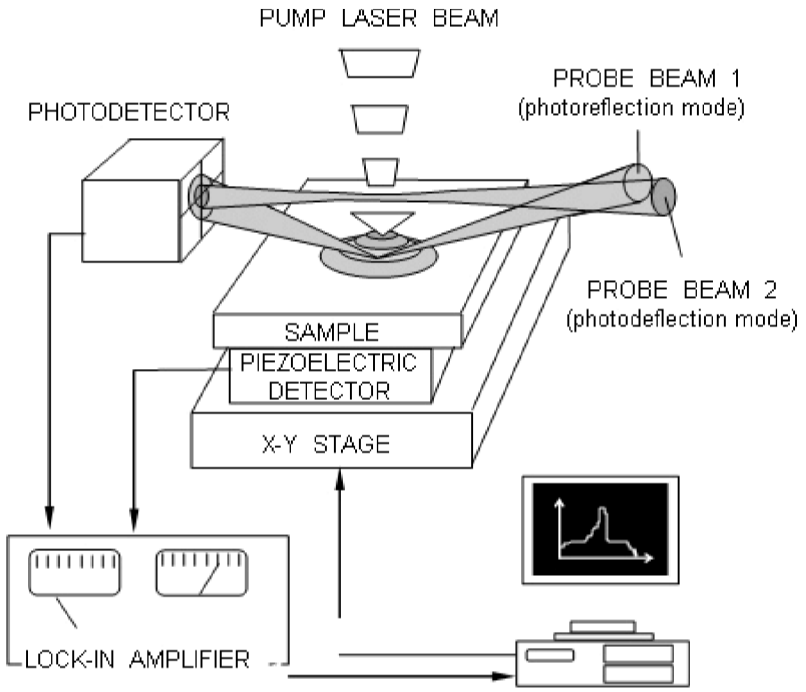

Fig. 1 The scheme of the set-up for the photothermal and photoacoustc microscopy of solids.

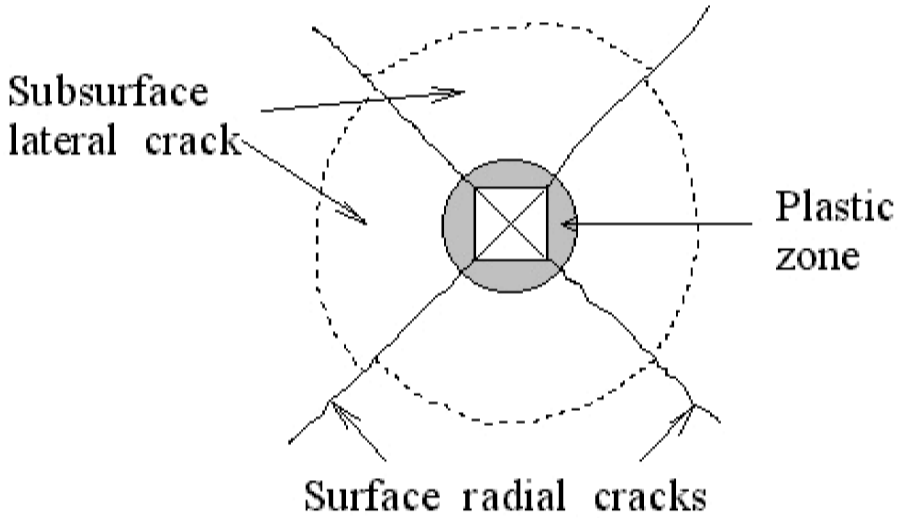

Fig. 2 Sketch of the Vickers indentation crack system for brittle solids. a is a top view, b is a cross section.

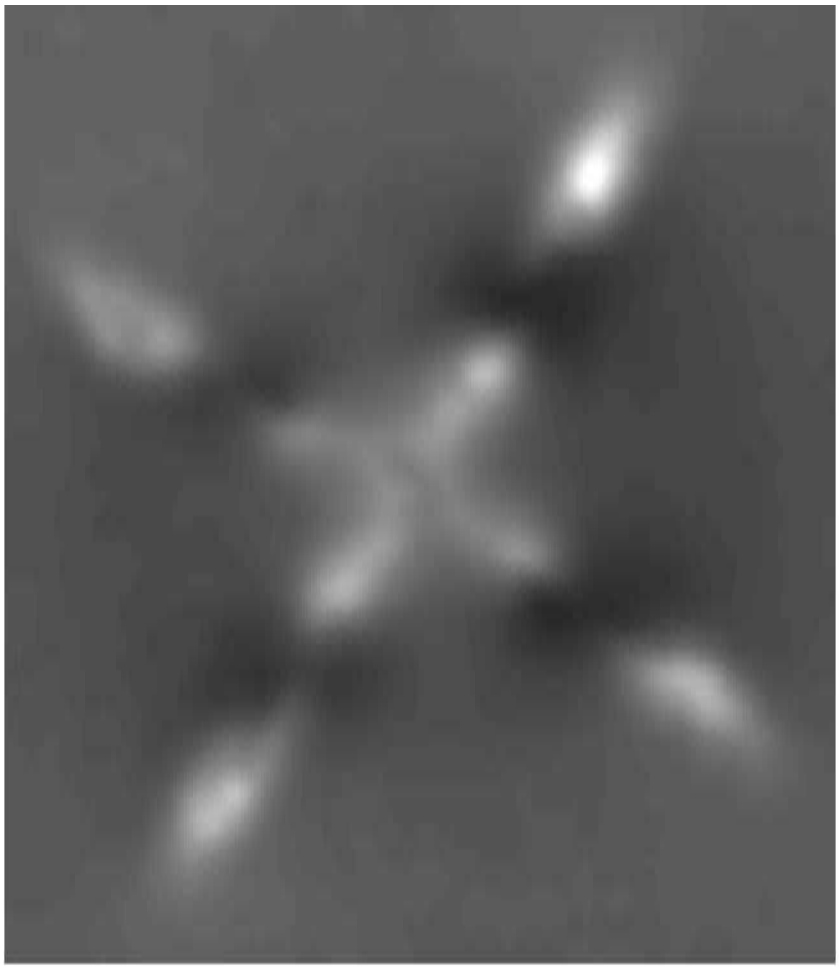

Fig. 3 The amplitude of the PA piezoelectric image of a Vickers indentation in Si_3N_4 ceramic. The indentation load is 98 N, the modulation frequency is 114 kHz, the image area is $370\times370\ \mu m^2$.

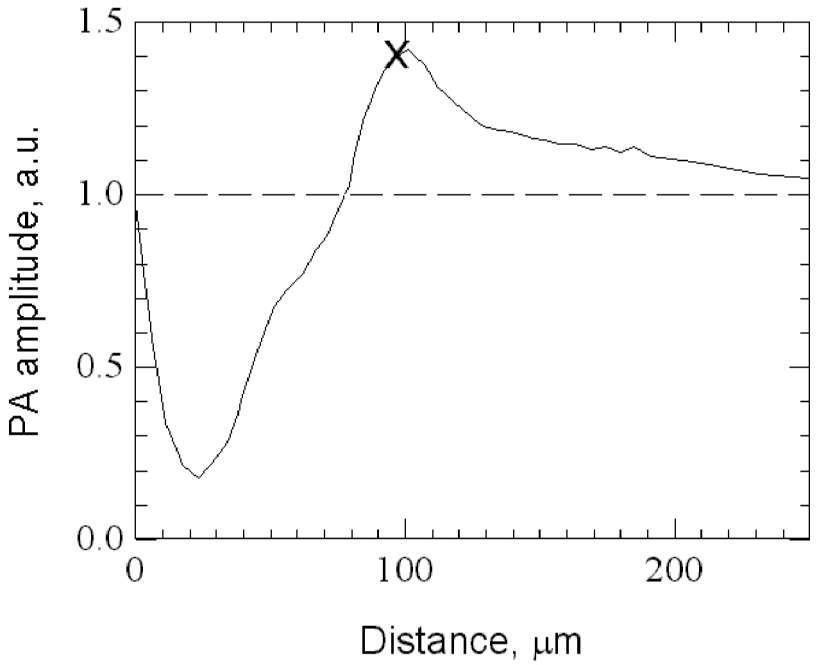

Fig. 4 The PA piezoelectric signal scan along a radial crack in Si_3N_4 ceramic. The indentation load is 98 N, the modulation frequency is 114 kHz. The distance is set equal to zero at the beginning of the crack.

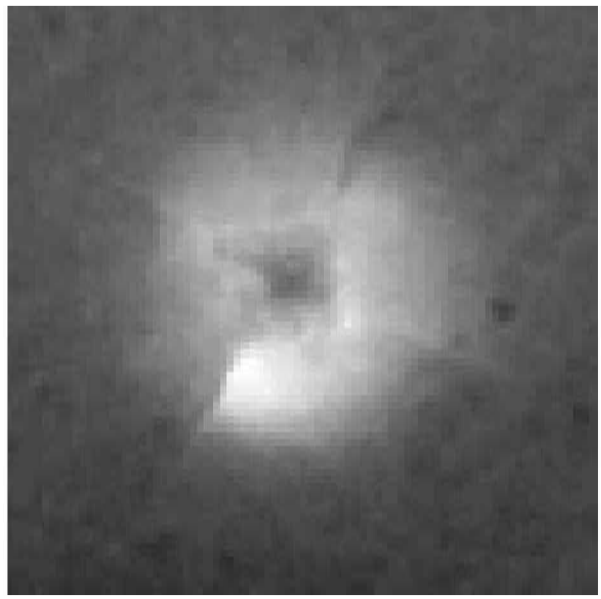

(a)

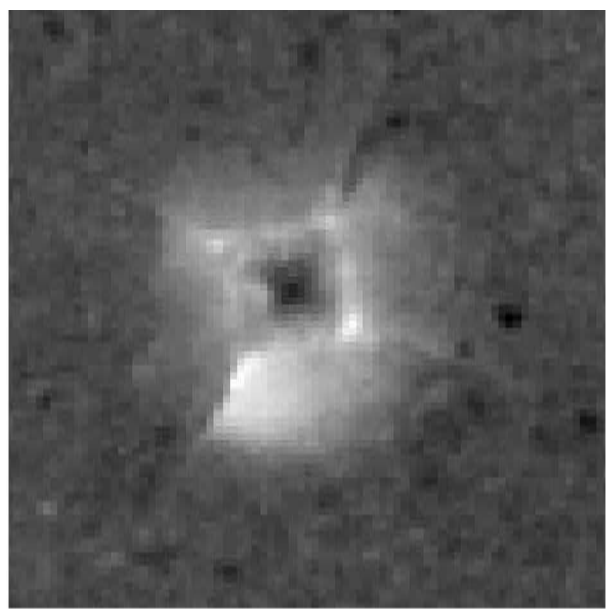

(b)

Fig. 5 The normal photodeflection image of a Vickers indentation in Si_3N_4 ceramic. The indentation load is 98 N, the modulation frequency is 7.6 kHz, the image area is 315×315 μm^2. (a): is a signal amplitude, (b): is a signal phase.

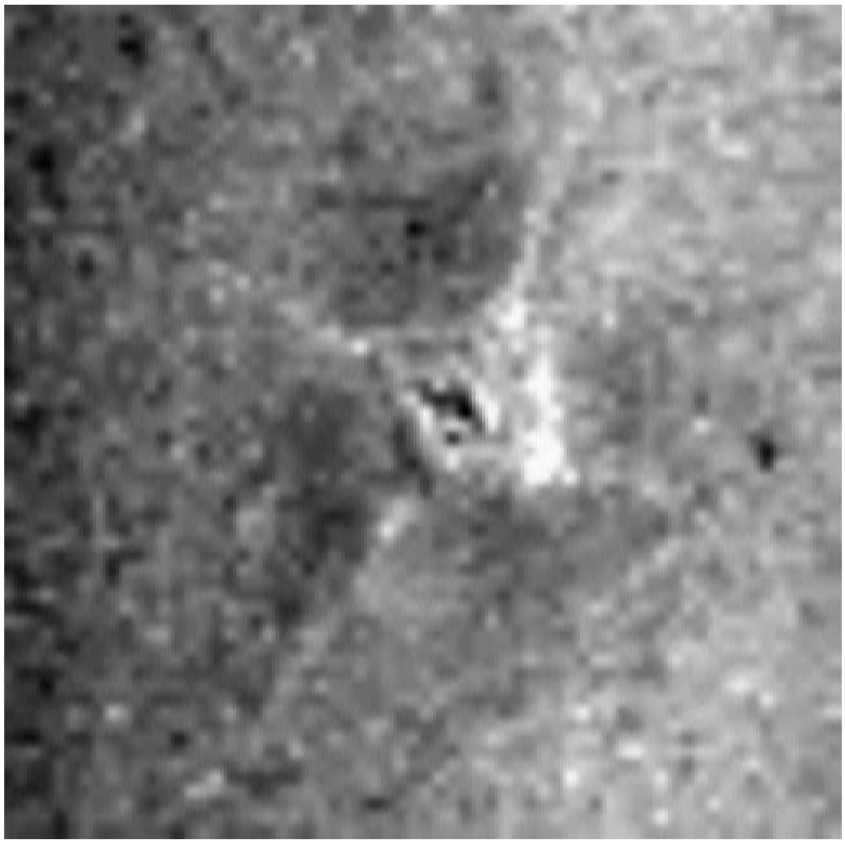

Fig. 6 The amplitude of the photoreflection image of a Vickers indentation in Si_3N_4 ceramic. The indentation load is 98 N, the modulation frequency is 7.6 kHz, the image area is 315×315 μm^2.

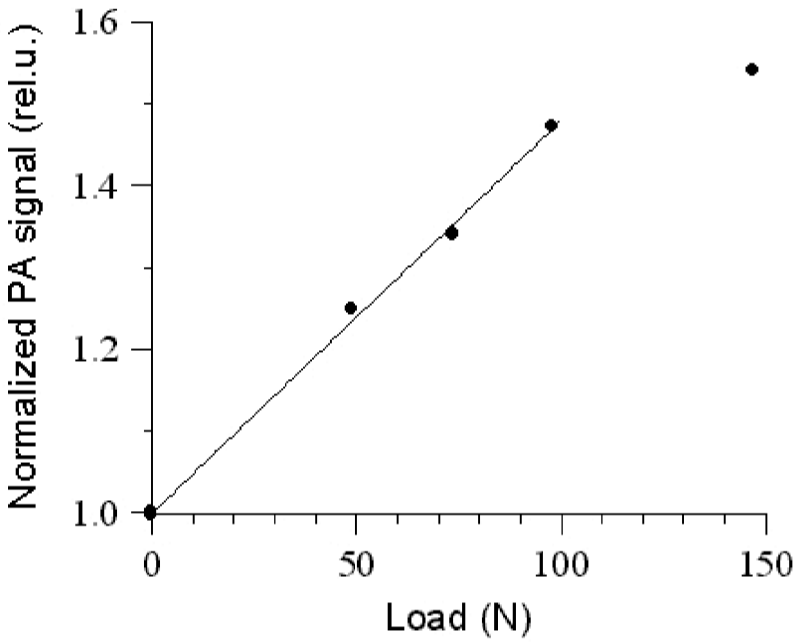

Fig. 7 The dependence of the maximum value of the PA piezoelectric signal on the indentation load for Si_3N_4 ceramic.

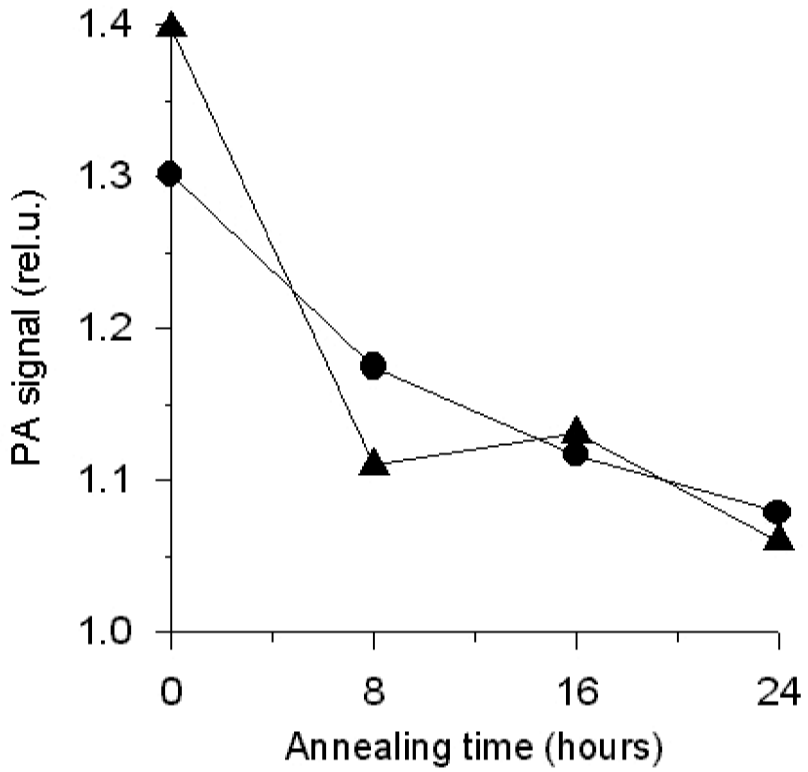

Fig. 8 The dependence of the maximal amplitude of the piezoelectric signal for Al_2O_3-SiC-TiC ceramic near the tips of two radial cracks on the annealing time.

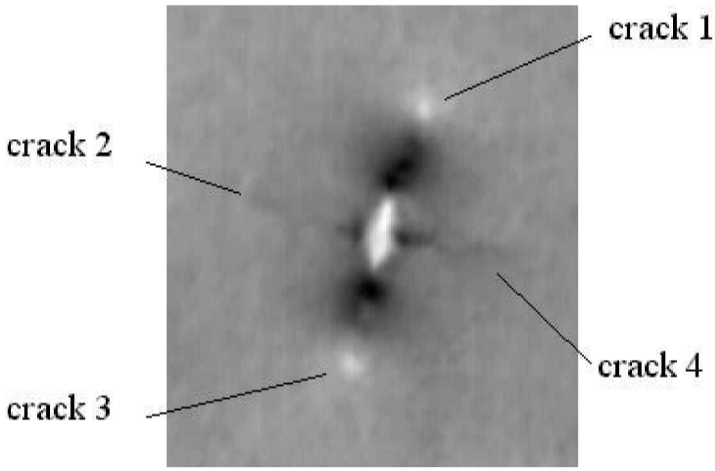

(a)

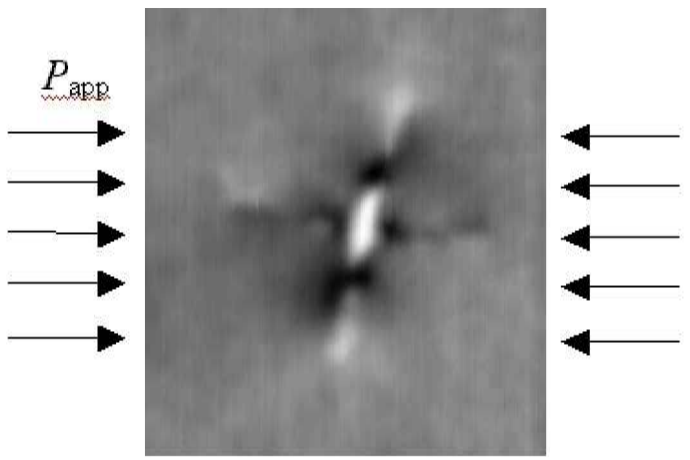

(b)

Fig. 9 The PA piezoelectric image of Vickers indentation in Al_2O_3-SiC-TiC ceramic. (a): without external load, (b): under the external loading of 170 MPa. The indentation load is 98 N, the modulation frequency is 142 kHz, the image area is 480×500 μm^2

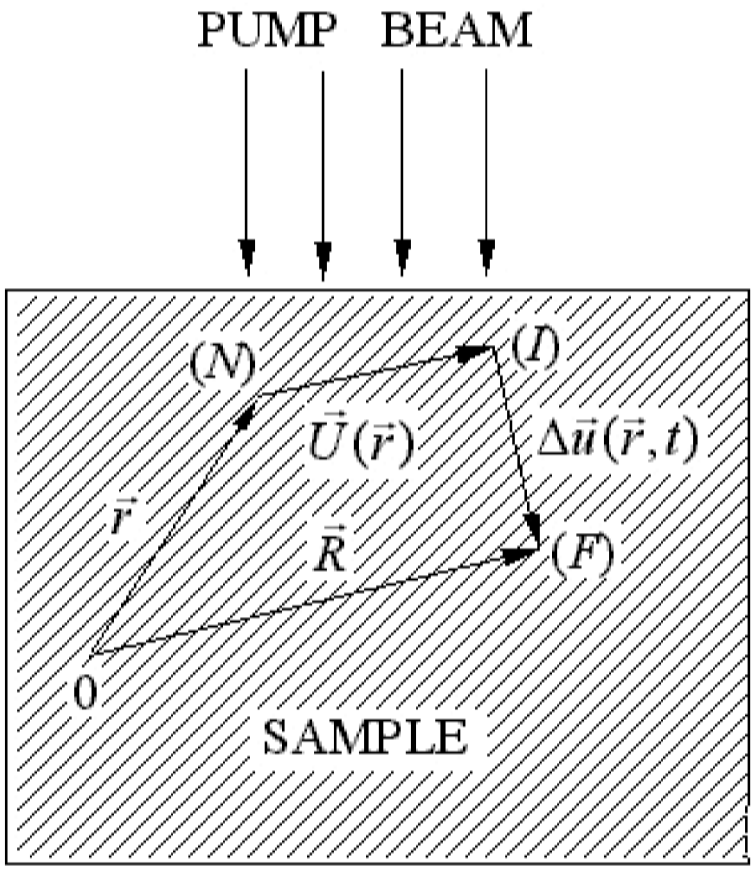

Fig. 10 Sketch of the three states of a sample irradiated by a pump beam. (N) is the natural state, (I) is the initial state, and (F) is the final state.

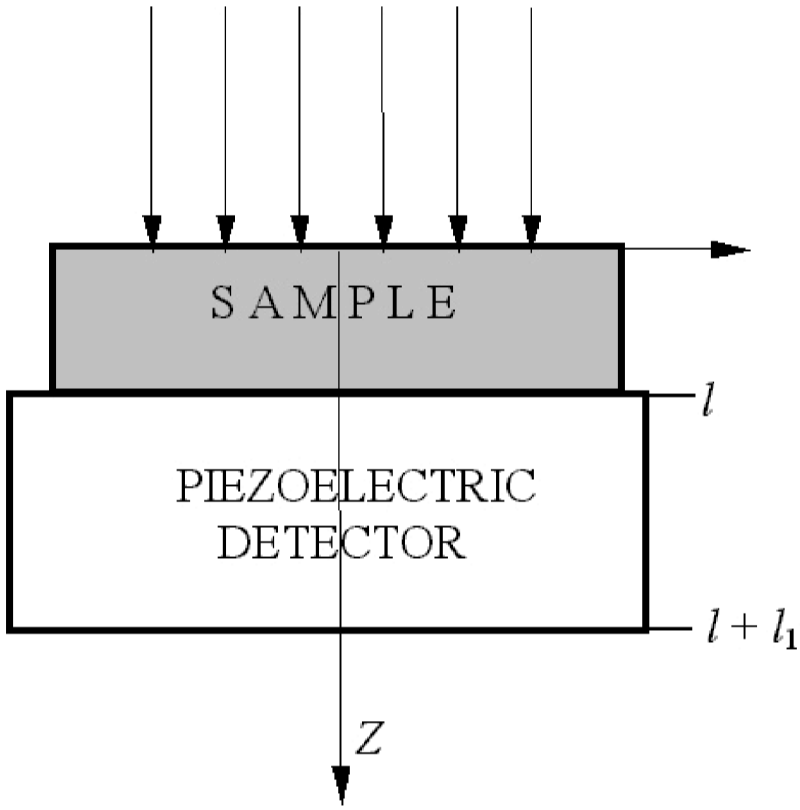

Fig. 11 Geometry of relative positions of a sample and a piezoelectric detector.

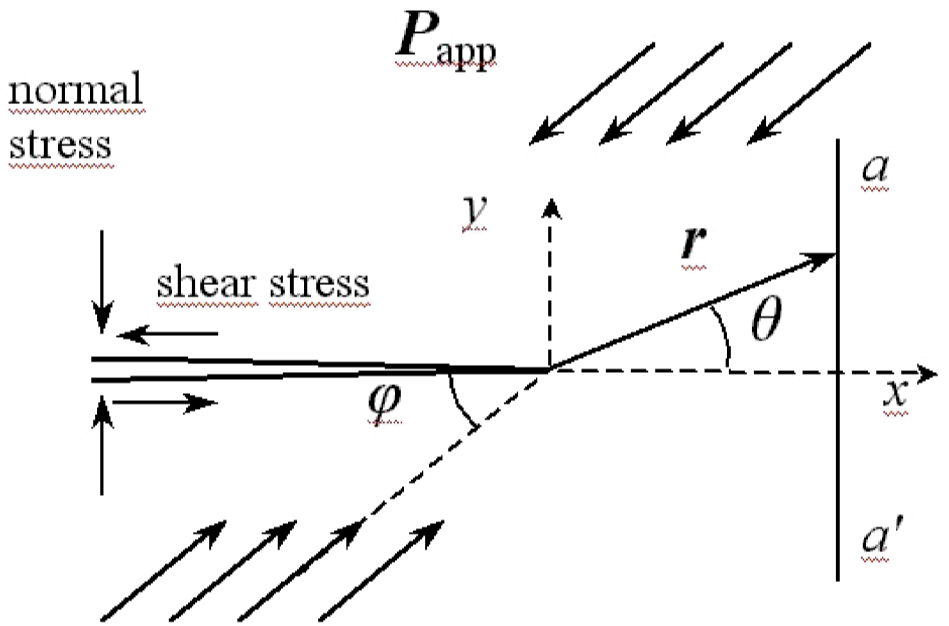

Fig. 12 The configuration of a crack and external loading.

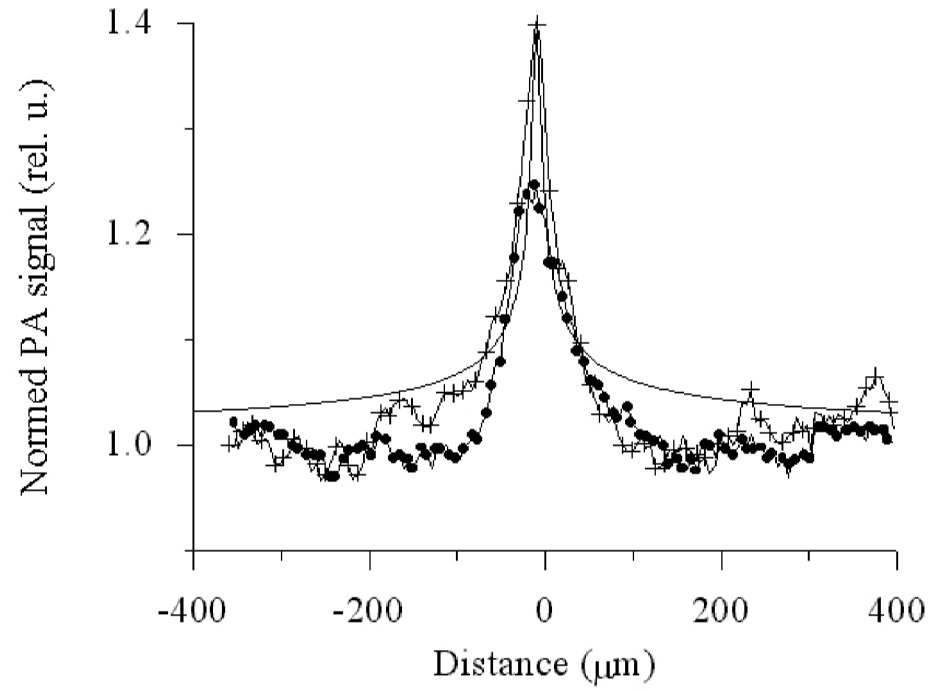

(a)

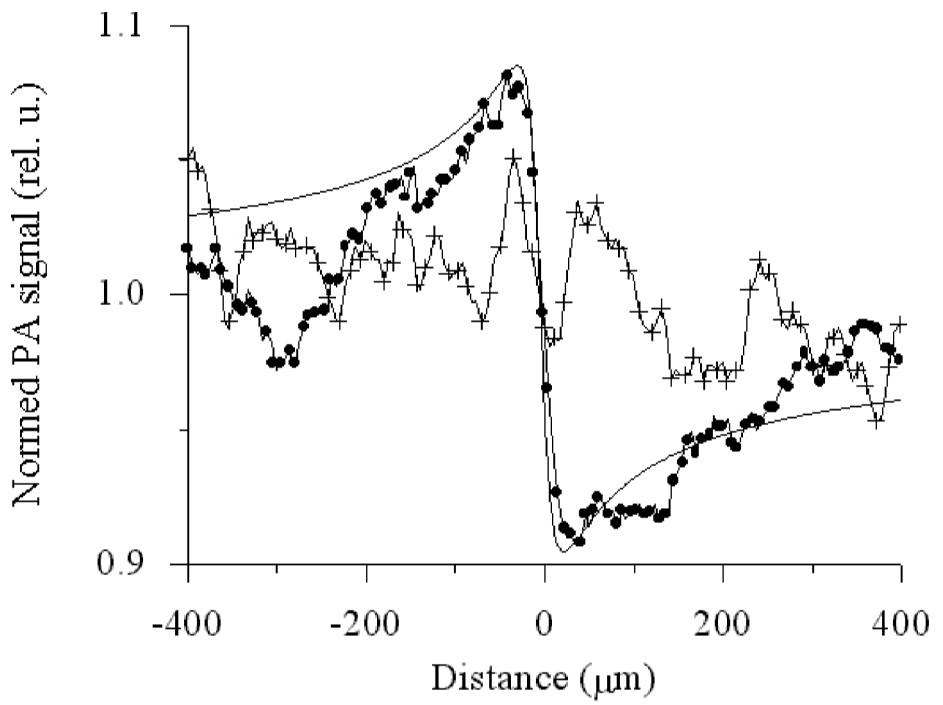

(b)

Fig. 13 The behavior of the PA piezoelectric signal near the radial crack tips in the direction across the cracks. (a): for crack 1, (b): for crack 4. + - experimental data for the sample without external loading, •- experimental data for the sample under the external loading of 170 MPa, ——— - theoretical curve.